RESEARCH ARTICLE

SYNTHETIC BIOLOGY

Engineering longevity—design of a synthetic gene oscillator to slow cellular aging

Zhen Zhou[1], Yuting Liu[1], Yushen Feng[1], Stephen Klepin[1], Lev S. Tsimring[2], Lorraine Pillus[1,3], Jeff Hasty[1,2,4], Nan Hao[1,2,4]*

Synthetic biology enables the design of gene networks to confer specific biological functions, yet it remains a challenge to rationally engineer a biological trait as complex as longevity. A naturally occurring toggle switch underlies fate decisions toward either nucleolar or mitochondrial decline during the aging of yeast cells. We rewired this endogenous toggle to engineer an autonomous genetic clock that generates sustained oscillations between the nucleolar and mitochondrial aging processes in individual cells. These oscillations increased cellular life span through the delay of the commitment to aging that resulted from either the loss of chromatin silencing or the depletion of heme. Our results establish a connection between gene network architecture and cellular longevity that could lead to rationally designed gene circuits that slow aging.

The era of genomic sequencing has generated a huge body of knowledge that defines molecular components and interactions within gene networks that control cellular functions. However, further advances in understanding how these networks confer biological functions have been hindered by the complexity of related regulatory interactions (*1*). One strategy in synthetic biology is to build simple orthogonal networks analogous to the core parts of natural systems that can be used to uncover key design principles of biological functions embedded in sophisticated network connections (*2*, *3*). For example, synthetic networks have been constructed to enable specific dynamic behaviors or functions, such as toggle switches, genetic oscillators, cellular counters, homeostasis, and multistability (*4*–*12*). As technologies for engineering biological systems improve rapidly, synthetic biology also offers a powerful approach to rewire and perturb intricate endogenous networks and to interrogate the relationship between network structure and cellular functions (*3*, *13*–*19*). In this work, we engineered an oscillatory gene network that effectively promotes the longevity of the cell.

Cellular aging is a fundamental and complex biological process that is an underlying driver for many diseases (*20*). We studied replicative aging of the yeast *Saccharomyces cerevisiae*, which has proven to be a genetically tractable model for the aging of mitotic cell types such as stem cells and has led to the identification of well-conserved genetic factors that influence longevity in eukaryotes (*21*–*26*). For example, the lysine deacetylase Sir2 and heme-activated protein (HAP) complex are deeply conserved, well-characterized transcriptional regulators that control yeast aging and life span. Sir2 mediates chromatin silencing at ribosomal DNA (rDNA) to maintain the stability of this fragile genomic locus and the integrity of the nucleolus (*27*–*30*). HAP regulates the expression of genes that are important for heme biogenesis and mitochondrial function (*31*).

To track rDNA silencing during aging of wild-type (WT) yeast cells, we used a green fluorescent protein (GFP) reporter inserted at the rDNA locus (rDNA-GFP). Its expression and fluorescence reflect the state of rDNA silencing: decreased fluorescence indicates enhanced silencing (*32*). To track heme abundance, we used a nuclear-anchored infrared fluorescent protein (nuc. iRFP), the fluorescence of which depends on biliverdin, a product of heme catabolism, and correlates with the abundance of cellular heme (*33*, *34*). To observe these two reporters, we used microfluidics coupled with time-lapse microscopy of single cells. We saw that isogenic WT cells age toward two discrete terminal states (*34*): one with decreased rDNA silencing [Fig. 1A (red dots) and fig. S1A], which leads to nucleolar enlargement and fragmentation (*34*), and one with decreased heme abundance [Fig. 1A (blue dots) and fig. S1B) and hence, mitochondrial aggregation and dysfunction (*34*). We further identified a mutual inhibition circuit of Sir2 and HAP that resembles a toggle switch and drives cellular fate decisions and commitment to either of these two detrimental states, contributing to cell deterioration and aging (*34*) (Fig. 1B).

Design of a synthetic oscillator for longevi

We considered the possibility of altering the Sir2-HAP circuit to reprogram aging trajectories toward a longer life span. Specifically, the introduction of a synthetic negative feedback loop between Sir2 and HAP could lead to sustained oscillations in the abundance of these two factors (Fig. 1C). Such periodic cycling might enable a dynamic balance in Sir2 and HAP during aging, avoiding a prolonged duration or cell-fate commitment to either rDNA silencing–loss or a heme-depletion state, and thus slow cell deterioration and extend life span.

To guide our network engineering, we devised a simple computational model to generate design specifications. The model consisted of positive transcriptional regulation of *SIR2* by HAP and Sir2-mediated transcriptional repression of HAP, which formed a delayed negative feedback loop (fig. S2, A and B) (materials and methods). With appropriate parameter values, the model generated sustained limit-cycle oscillations (Fig. 1C and fig. S2C). We used Monte Carlo simulations to systematically explore the parameter space and to analyze the dependence of sustained oscillatory behaviors on the parameter values (fig. S3A). Oscillations were favored by strong HAP-activated transcription of *SIR2*, high capacity of transcription of HAP, and tight transcriptional repression of HAP by Sir2 (fig. S3). We therefore focused our engineering efforts on fulfilling these specifications.

To enable strong positive transcriptional regulation of *SIR2* by HAP, we replaced the native promoter of *SIR2* with a *CYC1* (Cytochrome C1) promoter, which is bound and activated by HAP (*35*–*37*). To monitor dynamic behaviors of the engineered circuit, *SIR2* was C-terminally tagged with the fluorescent reporter protein mCherry, which did not affect cell growth or aging (fig. S4). To ensure a high capacity for transcription of HAP, we built a construct that contained the *HAP4* gene, encoding a major component of the HAP complex, under a strong, constitutive *TDH3* (triosephosphate dehydrogenase 3) promoter. To enable dynamic transcriptional repression of HAP by Sir2, we integrated the *HAP4* construct at the nontranscribed spacer (NTS) region within the rDNA, which is subject to transcriptional silencing mediated by Sir2 (*29*, *38*) (Fig. 1D). The endogenous copy of *HAP4* was deleted in the synthetic strain to minimize leakiness of *HAP4* expression. We did not tag *HAP4* with a fluorescent reporter because its protein abundance is below the detection limit of fluorescence microscopy. These regulatory parts were selected based on the model-guided design specifications: The *CYC1* promoter and transcriptional silencing at rDNA were selected because both were previously characterized to have low leakiness (*36*, *39*). We selected the *TDH3* promoter to

[1]Department of Molecular Biology, University of California San Diego, La Jolla, CA 92093, USA. [2]Synthetic Biology Institute, University of California San Diego, La Jolla, CA 92093, USA. [3]UCSD Moores Cancer Center, University of California San Diego, La Jolla, CA 92093, USA. [4]Department of Bioengineering, University of California San Diego, La Jolla, CA 92093, USA.
*Corresponding author. Email: nhao@ucsd.edu

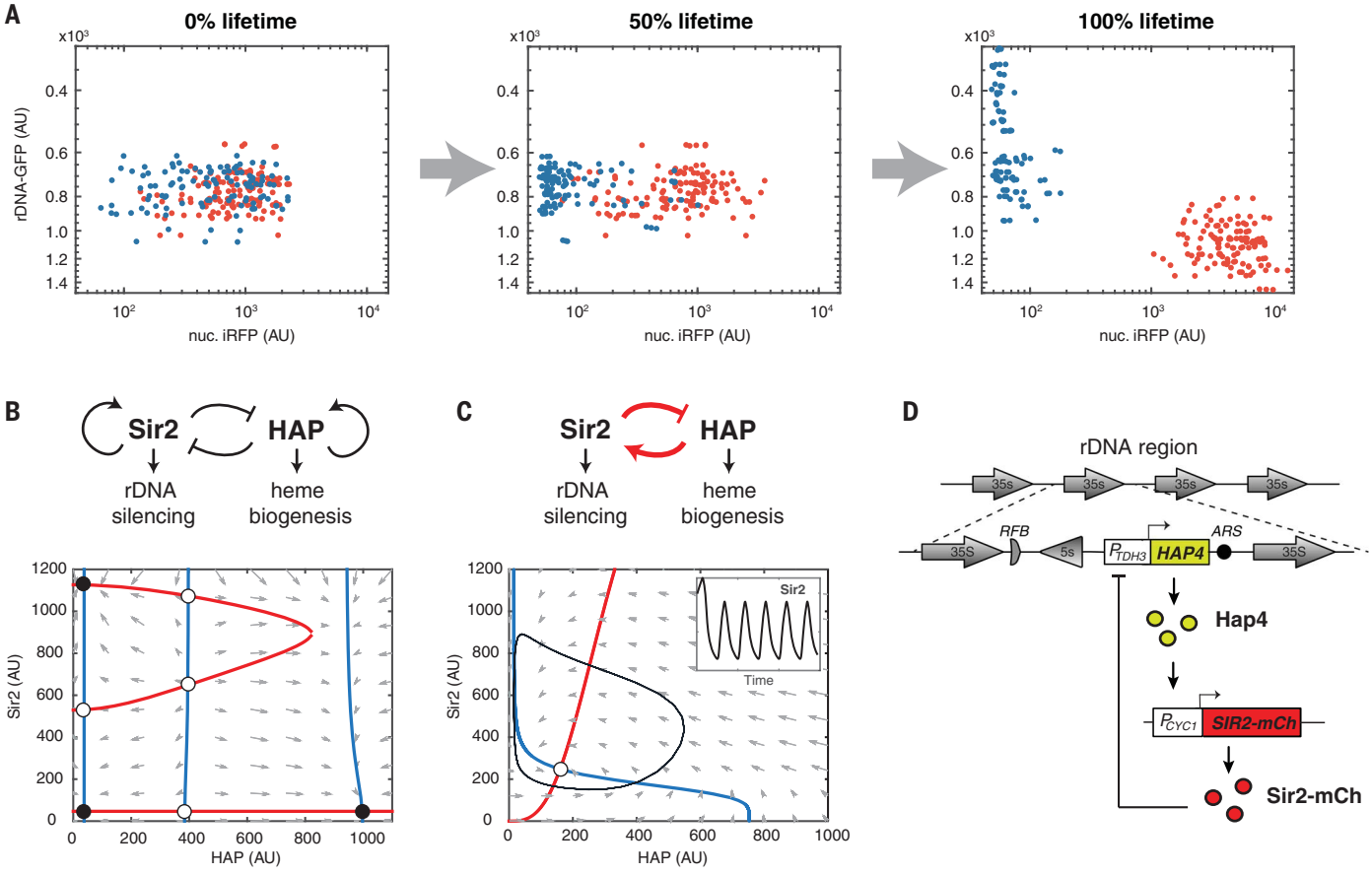

Fig. 1. Construction of a synthetic gene oscillator to reprogram aging. (**A**) Divergent aging in isogenic WT cells. Dot plots show the distributions of rDNA-GFP and nuc. iRFP reporter fluorescence in single cells tracked by time-lapse microscopy of single cells over the course of their life spans. Each dot represents a single cell monitored individually in a microfluidic chamber. The red dots represent aging with rDNA silencing–loss, indicated by increased rDNA-GFP fluorescence. The blue dots represent aging with heme depletion, indicated by decreased iRFP fluorescence. Experiments were independently performed at least three times. AU, arbitrary units. (**B**) The endogenous Sir2-HAP circuit and its simulated dynamic behaviors in WT aging. (Top) Diagram of the circuit topology. (Bottom) Phase plane diagram illustrating the dynamic changes of Sir2 and HAP activities during aging. The nullclines of Sir2 and HAP are represented in red and blue, respectively. The quivers represent the rate and direction of the movement of the system. Fixed points are indicated with open (unstable) and closed (stable) circles. The stable fixed point on the bottom right corresponds to the terminal states of aging cells undergoing rDNA silencing–loss and nucleolar decline [(red dots in (A)]; the stable fixed points on the left correspond to the terminal states of aging cells undergoing heme depletion and mitochondrial decline [blue dots in (A)]. (**C**) The rewired Sir2-HAP circuit and its dynamic behaviors. (Top) Circuit topology with the synthetic negative feedback loop in red. (Bottom) Phase plane diagram with a limit cycle (black line) arising from the circuit, in which Sir2 and HAP periodically change their levels. (Inset) Simulated time traces of oscillatory Sir2 expression. (**D**) A schematic illustrates the construction of the synthetic circuit. The native promoter of *SIR2* was replaced with a HAP-inducible *CYC1* promoter (P_{CYC1}). *HAP4* under a strong, constitutive *TDH3* promoter (P_{TDH3}) was inserted at the rDNA locus, which is subject to transcriptional silencing mediated by Sir2.

drive *HAP4* expression because it is one of the strongest constitutive promoters in yeast (*40*, *41*).

Sustained oscillations during aging

We used microfluidics coupled with time-lapse microscopy to track dynamic changes in Sir2-mCherry fluorescence throughout the life span of single cells. Engineered cells (n = 113) exhibited oscillations in abundance of Sir2 during aging (Fig. 2A, fig. S5, and movie S1). WT control cells (n = 93) did not show such oscillations (Fig. 2A and fig. S5). We quantified the amplitude and period of oscillatory pulses in the engineered cells (fig. S6). The average amplitude of oscillations was 309 ± 108 arbitrary units (Fig. 2B), which was much larger than fluctuations in WT cells (36 ± 30 AU). The average period was 557 ± 151 min (Fig. 2C), longer than the typical cell doubling times (~90 to 120 min), which indicates that the oscillations were not driven by cell cycle. We also performed spectral analysis of Sir2 time traces (fig. S7). For the engineered strain, we could clearly see a spectral power peak around frequency 2.33×10^{-5} Hz corresponding to a period of 12 hours. By contrast, the spectrum of WT was flat and white noise–like, without a clear peak (fig. S7B).

Oscillations in the synthetic strain were heterogeneous among individual cells. Of the engineered cells, 65% exhibited sustained oscillations throughout their entire life spans, whereas 35% deviated from oscillations late in their life spans and showed increased accumulation of Sir2 before cell death (Fig. 2D and fig. S8). This deviation might arise from an age-induced decrease in Sir2-mediated silencing activity (*32*, *42*, *43*) in some cells, which could lead to increased HAP expression from the rDNA locus and in turn, a continuous increase in Sir2 expression driven by HAP.

During the process of circuit engineering, we also constructed and characterized versions of the synthetic circuit with broken or weakened feedback interactions. These include (i) a circuit without HAP-activated expression of Sir2; (ii) a circuit without Sir2-mediated

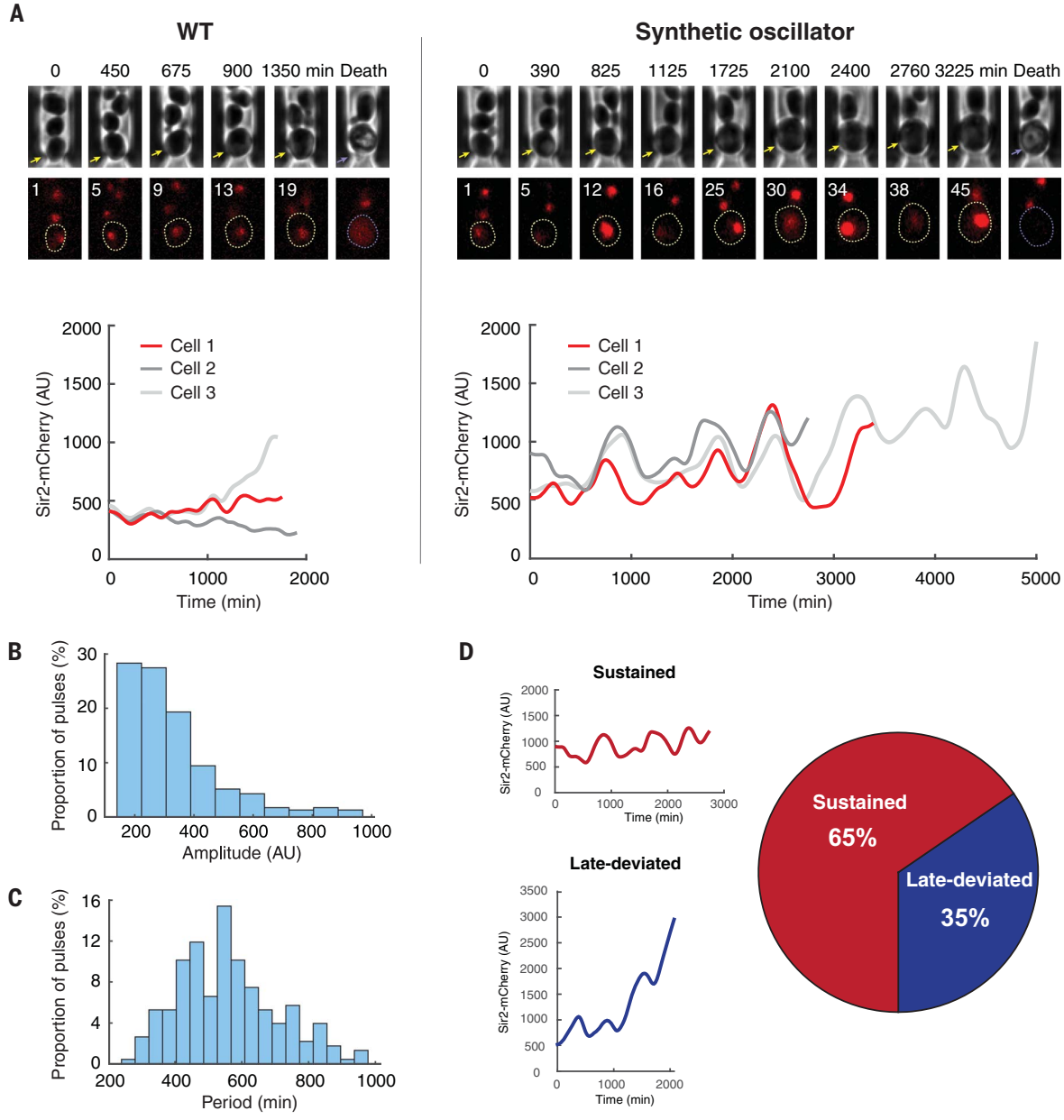

Fig. 2. Oscillations in the synthetic strain during aging. (**A**) Dynamics of Sir2-mCherry fluorescence in WT (left) and the synthetic strain (right) during aging. (Top) Representative time-lapse images for phase and Sir2-mCherry from single aging cells in the microfluidic chamber. For phase images, aging and dead mother cells are represented by yellow and purple arrows, respectively. In fluorescence images, replicative age of the mother cell is shown at the top left corner of each image: aging and dead mother cells are circled in yellow and purple, respectively. (Bottom) Fluorescence time traces throughout the life spans of representative cells. The time trace in red corresponds to the time-lapse images shown above the plot. Time traces of all the cells measured are included in fig. S5. (**B**) Distribution of the amplitudes of Sir2 oscillatory pulses in the engineered cells. (**C**) Distribution of the periods of Sir2 oscillatory pulses in the engineered cells. Panels (B) and (C) show distributions of single pulses. The quantification of amplitude and period is included in the materials and methods and fig. S6. (**D**) Proportions of aging cells from the synthetic strain that show sustained oscillations (Sustained) or a deviation from oscillation late in life (Late-deviated) (n = 113). (Left) Representative time traces for sustained oscillation (top) and late deviation from oscillation (bottom). The stability determination for Sir2 oscillations is available in the materials and methods and fig. S8. Experiments were independently performed at least three times.

repression of HAP; and (iii) a circuit with a weaker transcriptional capacity of HAP. None of these circuits enabled sustained oscillations in a major fraction of cells (fig. S9), which demonstrated the importance of connectivity and strength of feedback interactions in generating oscillations.

The synthetic oscillator extends life span

The synthetic oscillator strain indeed showed an 82% increase in life span compared to that of WT control cells (Fig. 3A). This is the most pronounced life-span extension in yeast that we have observed with genetic perturbations. Among the engineered cells, those aging with sustained oscillations had greater life-span extension (105% increase in life span, doubling that of WT) than those that deviated from oscillations late in life (45% increase relative to that of WT) (Fig. 3A, red versus blue dashed curves). Thus, maintaining Sir2 oscillation appears to be important for maximally extending life span.

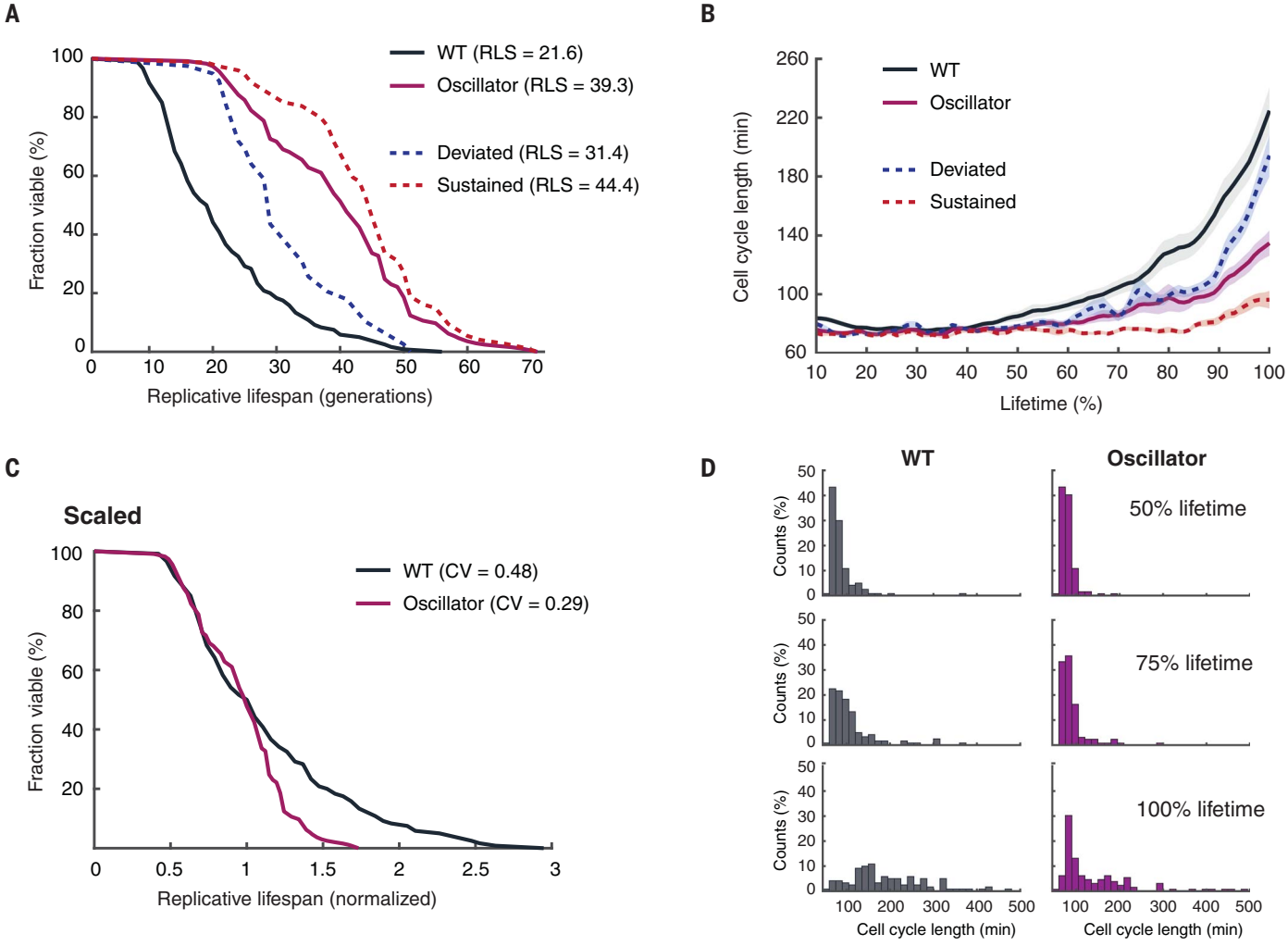

Fig. 3. Life-span extension by the synthetic oscillator. (**A**) Replicative life spans for WT (black, *n* = 131 cells) and the synthetic oscillator strain (purple, *n* = 120 cells). Among the cells in the synthetic oscillator strain, the life spans for those that deviated from oscillations (*n* = 39 cells) and those with sustained oscillations (*n* = 74 cells) were shown as blue and red dashed curves, respectively. $P < 0.0001$ with Gehan-Breslow-Wilcoxon test. (**B**) Changes of cell cycle length during aging for WT (black), the synthetic oscillator strain (purple), the oscillator cells that deviated from oscillations (blue dashed curve), and the oscillator cells with sustained oscillations (red dashed cells). Shaded areas represent standard errors of the mean (SEM). (**C**) The life-span curves for WT and the synthetic oscillator strain, scaled by the median. The CV of life spans among cells was calculated for WT and the synthetic oscillator strain. (**D**) The histograms represent distributions of cell cycle lengths at different stages of aging for WT and the synthetic oscillator strain. Experiments were independently performed at least three times.

The synthetic oscillator strain exhibited a fast cell cycle rate and the elongation of cell cycles during aging was delayed and decreased compared to that in WT cells (Fig. 3B). Engineered cells with sustained oscillations retained a fast cell cycle rate (70 to 90 min per cell cycle) throughout their entire life spans, whereas those that deviated from oscillations had much slower cell cycles late in life (Fig. 3B, red vs blue dashed curves). Thus, maintaining Sir2 oscillation appears to slow age-induced cell deterioration.

WT cells show a large cell-to-cell variation in life span (coefficient of variation (CV) = 0.48), in part because of the stochasticity and divergence of the Sir2 and HAP deterioration pathways (*34*). The synthetic negative feedback loop in our engineered strain could function to avoid or delay such pathway divergence. In agreement with this, the synthetic oscillator strain showed a more uniform life span among cells (CV = 0.29) and less increase in cell cycle length during aging compared to WT (Fig. 3, C and D).

In the synthetic oscillator strain, the abundance of Sir2, averaged over the lifetime, was elevated by about twofold relative to that of WT (fig. S10). To test whether the life-span extension is simply because of the increased Sir2 abundance, we examined the strain with twofold constitutive overexpression of Sir2. We observed a ~23% increase in life span compared to WT (fig. S11A). Twofold overexpression of Sir2 in combination with Hap4 overexpression resulted in a more notable life-span extension (~42% increase compared to WT), which was still substantially less than the life-span extension from the oscillator strain (82% increase compared to WT) (fig. S11). The oscillator strain also has a faster cell cycle rate than the overexpression mutants (fig. S11C). These results confirm that the oscillatory dynamics of Sir2, in addition to its increased expression, contribute to the life span extension and fast cell cycle rate in the synthetic strain. In line with this, the oscillator strain is also much more long-lived than strains with engineered Sir2-HAP circuits that cannot generate oscillations because of broken or weakened feedback interactions (fig. S12).

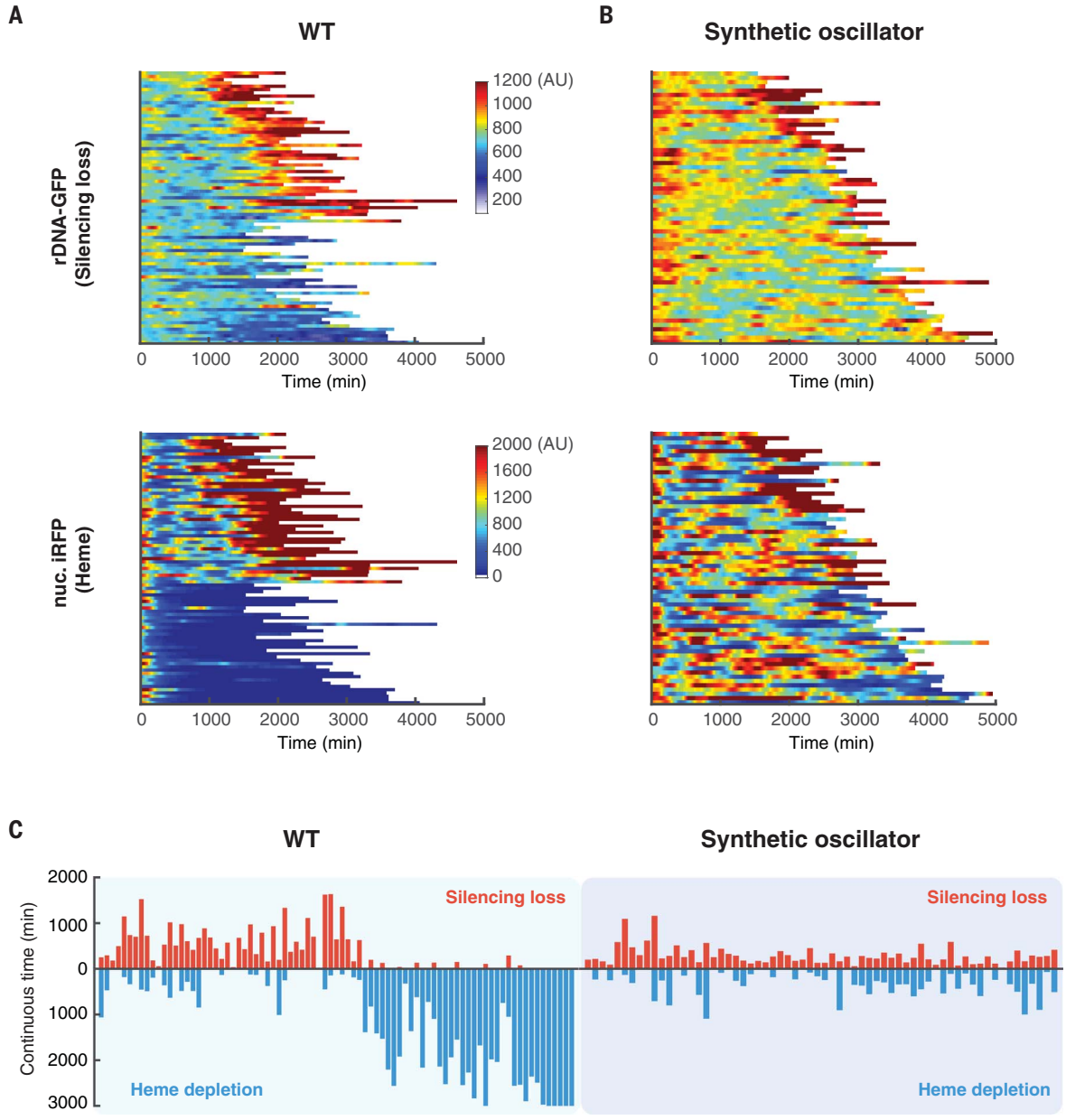

Fig. 4. The synthetic oscillator maintains a balance between rDNA silencing and heme biogenesis. (**A**) Single-cell color map trajectories of rDNA-GFP (top) and nuclear-anchored iRFP (bottom) in WT aging cells (n = 83). Each row represents the time trace of a single cell throughout its life span. Color represents the fluorescence intensity as indicated in the color bar. Color maps for rDNA-GFP and iRFP are from the same cells with the same top-to-bottom order. Cells are classified into two groups. Those in the top half of the color maps are WT cells that showed continuous high GFP and iRFP signals, which indicated rDNA silencing–loss and high heme abundance at the later stage of life span. These cells also produced elongated daughters at the later stage of life span and were previously designated as "mode 1" aging (*34*). Those in the bottom half of the color maps are WT cells that showed constantly or gradually decreased GFP fluorescence and sharply decreased iRFP fluorescence, which indicated high rDNA silencing and heme depletion at the late stage of aging. These cells produced small round daughters throughout the life span, previously designated as "mode 2" aging (*34*). (**B**) Single-cell color map trajectories of rDNA-GFP (top) and nuc. iRFP (bottom) in aging cells of the synthetic oscillator strain (n = 64). Color maps for rDNA-GFP and iRFP are from the same cells. Color maps used the same color bars as those in (A). (**C**) Bar graphs showing continuous times of the rDNA silencing–loss or heme-depletion state for WT (left) and the synthetic oscillator strain (right). Each bidirectional bar represents a single cell, in which the red upward portion indicates its continuous time of the rDNA silencing–loss state, and the blue downward portion indicates the continuous time of the heme depletion-state. The graphs were quantified using the data from (A) and (B) (fig. S14) (materials and methods). Experiments were independently performed at least three times.

To further assess the performance of the synthetic oscillator strain, we compared it with longest-lived single and double mutants identified from genetic screens (*44*–*46*). These include the deletion mutants *fob1*Δ ("forkblocking less," which encodes a protein required for replication fork blocking), *sgf73*Δ (SAGA-associated factor 73, which encodes a component of the SAGA/SLIK complex deubiquitination module), *fob1*Δ *hxk2*Δ (the double mutant of genes that encode forkblocking less and hexokinase 2), and *fob1*Δ *sch9*Δ (the double mutant of genes

that encode forkblocking less and an ortholog of the mammalian S6 kinase). Under the genetic background and experimental conditions we used (materials and methods) (*32*, *34*, *47*), the synthetic oscillator strain had a longer and more uniform life span than most mutants (fig. S13, A and B). Moreover, some longevity mutants displayed impaired cell cycle progression even in young cells, which suggests moderate physiological defects associated with the genetic perturbations. In contrast, the oscillator strain had faster cell cycles than WT and mutants throughout the entire aging process, which indicated a healthier cellular life span (fig. S13C).

The synthetic oscillator avoids fate commitment to deterioration states

To test whether sustained oscillations in the engineered Sir2-HAP circuit could prevent aging cells from committing to either the rDNA silencing–loss or heme-depletion state, we simultaneously monitored rDNA silencing and heme abundance in the synthetic strain with the rDNA-GFP and iRFP reporters.

In accordance with previous results (*34*), in WT cells, about half of the cells showed continuously increased GFP fluorescence at the later stages of aging, which indicated a sustained loss of rDNA silencing and ended life in a state with low rDNA silencing and a high abundance of heme. The other cells showed decreased iRFP fluorescence, which indicated that heme was depleted, and ended life in a state with high rDNA silencing and a low abundance of heme (Fig. 4A). In contrast, most synthetic oscillator cells exhibited short, intermittent pulses of rDNA-GFP and iRFP signals throughout the life span without a prolonged commitment to either a state of rDNA silencing–loss or of heme depletion (Fig. 4B). We further quantified the continuous times in the states of rDNA silencing–loss and heme depletion during the aging of each individual cells (fig. S14). Almost all of WT aging cells experienced a prolonged duration in rDNA silencing loss or heme depletion, whereas the oscillator cells showed shorter durations in either state (Fig. 4C and fig. S15). Thus, the engineered negative feedback loop in the Sir2-HAP circuit enabled a time-based balance between rDNA silencing and heme biogenesis that promoted longevity. In further support of this balance, synthetic Sir2-HAP circuits with broken or weakened feedback interactions failed to maintain such a balance, which resulted in prolonged commitments to detrimental states (fig. S16) and thereby, shorter life spans (fig. S12).

Discussion

Most studies of aging focus on measuring life span as a static endpoint assay and on identifying genes whose deletion or overexpression affects life span. These investigations have led to the identification of many conserved genes that influence aging (*24*, *48*–*50*). Building on the knowledge of aging factors and pathways from genetic studies, we used engineering principles to rationally optimize aging dynamics toward extended longevity. Specifically, based on the understanding of Sir2 and HAP pathways in the aging of WT cells (*34*, *45*), we rewired their interactions into a negative feedback loop and created a gene oscillator that functions to maintain cellular homeostasis. This synthetic system is advantageous in its robustness and effectiveness on life-span extension over longevity mutants from genetic screens and simple overexpression of Sir2, HAP, or both (fig. S17). The overexpression of longevity factors such as Sir2 or HAP led to variations in gene expression that inevitably drive cell fate commitment and deterioration in a fraction of cells (fig. S18), leading to short-lived cell subpopulations (*34*). Moreover, through this synthetic biology study, we established a causal connection between gene network architecture and longevity and further validated the mechanistic understanding of aging in the natural system.

The use of engineering principles to modulate biological functions is one of the major goals of synthetic biology (*2*, *3*). Many studies have succeeded in generating specific spatiotemporal dynamics and functions with synthetic gene circuits, yet it remains a challenge to rationally engineer a biological trait as complex as longevity. Our work represents a proof-of-concept, demonstrating the successful application of synthetic biology to reprogram the cellular aging process, and may lay the foundation for designing synthetic gene circuits to effectively promote longevity in more complex organisms.

REFERENCES AND NOTES

1. R. Milo *et al*., *Science* **298**, 824–827 (2002).
2. M. Elowitz, W. A. Lim, *Nature* **468**, 889–890 (2010).
3. C. J. Bashor, J. J. Collins, *Annu. Rev. Biophys.* **47**, 399–423 (2018).
4. T. S. Gardner, C. R. Cantor, J. J. Collins, *Nature* **403**, 339–342 (2000).
5. M. B. Elowitz, S. Leibler, *Nature* **403**, 335–338 (2000).
6. J. Stricker *et al*., *Nature* **456**, 516–519 (2008).
7. A. E. Friedland *et al*., *Science* **324**, 1199–1202 (2009).
8. T. Danino, O. Mondragón-Palomino, L. Tsimring, J. Hasty, *Nature* **463**, 326–330 (2010).
9. A. Becskei, L. Serrano, *Nature* **405**, 590–593 (2000).
10. R. Zhu, J. M. Del Rio-Salgado, J. Garcia-Ojalvo, M. B. Elowitz, *Science* **375**, eabg9765 (2022).
11. F. Wu, R. Q. Su, Y. C. Lai, X. Wang, *eLife* **6**, e23702 (2017).
12. M. Tigges, T. T. Marquez-Lago, J. Stelling, M. Fussenegger, *Nature* **457**, 309–312 (2009).
13. C. J. Bashor, A. A. Horwitz, S. G. Peisajovich, W. A. Lim, *Annu. Rev. Biophys.* **39**, 515–537 (2010).
14. F. Wu, J. H. Bethke, M. Wang, L. You, *Curr. Opin. Biomed. Eng.* **4**, 116–126 (2017).
15. L. Bintu *et al*., *Science* **351**, 720–724 (2016).
16. A. J. Keung, C. J. Bashor, S. Kiriakov, J. J. Collins, A. S. Khalil, *Cell* **158**, 110–120 (2014).
17. S. Toda, L. R. Blauch, S. K. Y. Tang, L. Morsut, W. A. Lim, *Science* **361**, 156–162 (2018).
18. S. Huang *et al*., *Mol. Syst. Biol.* **12**, 859 (2016).
19. A. H. Ng *et al*., *Nature* **572**, 265–269 (2019).
20. A. V. Belikov, *Ageing Res. Rev.* **49**, 11–26 (2019).
21. L. Fontana, L. Partridge, V. D. Longo, *Science* **328**, 321–326 (2010).
22. V. D. Longo, B. K. Kennedy, *Cell* **126**, 257–268 (2006).
23. B. M. Wasko, M. Kaeberlein, *FEMS Yeast Res.* **14**, 148–159 (2014).
24. M. Kaeberlein, B. K. Kennedy, *Mech. Ageing Dev.* **126**, 17–21 (2005).
25. C. He, C. Zhou, B. K. Kennedy, *Biochim. Biophys. Acta Mol. Basis Dis.* **1864** (9 Pt A), 2690–2696 (2018).
26. E. D. Smith *et al*., *Genome Res.* **18**, 564–570 (2008).
27. M. R. Gartenberg, J. S. Smith, *Genetics* **203**, 1563–1599 (2016).
28. M. Kaeberlein, M. McVey, L. Guarente, *Genes Dev.* **13**, 2570–2580 (1999).
29. K. Saka, S. Ide, A. R. Ganley, T. Kobayashi, *Curr. Biol.* **23**, 1794–1798 (2013).
30. D. A. Sinclair, L. Guarente, *Cell* **91**, 1033–1042 (1997).
31. S. Buschlen *et al*., *Comp. Funct. Genomics* **4**, 37–46 (2003).
32. Y. Li *et al*., *Proc. Natl. Acad. Sci. U.S.A.* **114**, 11253–11258 (2017).
33. G. S. Filonov *et al*., *Nat. Biotechnol.* **29**, 757–761 (2011).
34. Y. Li *et al*., *Science* **369**, 325–329 (2020).
35. J. Olesen, S. Hahn, L. Guarente, *Cell* **51**, 953–961 (1987).
36. L. Guarente, T. Mason, *Cell* **32**, 1279–1286 (1983).
37. S. Hahn, L. Guarente, *Science* **240**, 317–321 (1988).
38. C. Li, J. E. Mueller, M. Bryk, *Mol. Biol. Cell* **17**, 3848–3859 (2006).
39. C. M. Gallo, D. L. Smith Jr., J. S. Smith, *Mol. Cell. Biol.* **24**, 1301–1312 (2004).
40. B. Ho, A. Baryshnikova, G. W. Brown, *Cell Syst.* **6**, 192–205.e3 (2018).
41. L. Xiong *et al*., *Microb. Cell Fact.* **17**, 58 (2018).
42. W. Dang *et al*., *Nature* **459**, 802–807 (2009).
43. T. Smeal, J. Claus, B. Kennedy, F. Cole, L. Guarente, *Cell* **84**, 633–642 (1996).
44. M. A. McCormick *et al*., *Cell Rep.* **8**, 477–486 (2014).
45. M. Kaeberlein, K. T. Kirkland, S. Fields, B. K. Kennedy, *PLOS Biol.* **2**, e296 (2004).
46. M. Kaeberlein *et al*., *Science* **310**, 1193–1196 (2005).
47. M. Jin *et al*., *Cell Syst.* **8**, 242–253.e3 (2019).
48. L. Guarente, C. Kenyon, *Nature* **408**, 255–262 (2000).
49. M. Kuningas *et al*., *Aging Cell* **7**, 270–280 (2008).
50. M. A. McCormick *et al*., *Cell Metab.* **22**, 895–906 (2015).
51. Z. Zhou, zhoutopo/science_aging_model: science, Zenodo (2021).

ACKNOWLEDGMENTS

Funding: National Institutes of Health R01AG056440 (N.H., J.H., L.P., and L.S.T.); National Institutes of Health R01GM144595 (N.H., J.H., L.P., and L.S.T.); National Institutes of Health R01AG068112 (N.H.); and National Institutes of Health R01GM111458 (N.H.) **Author contributions**: Conceptualization: Z.Z., L.S.T., L.P., J.H., and N.H.; Methodology: Z.Z., Y.L., S.K., L.S.T., L.P., J.H., and N.H.; Investigation: Z.Z., Y.L., S.K., and Y.F.; Formal analysis: Z.Z., Y.L., and Y.F.; Funding acquisition: L.S.T., L.P., J.H., and N.H.; Project administration: N.H.; Supervision: N.H.; Writing – original draft: Z.Z. and N.H.; Writing – review and editing: Z.Z., Y.L., S.K., Y.F., L.S.T., L.P., J.H., and N.H. **Competing interests:** The authors declare that they have no competing interests. **Data and materials availability:** All data are available in the main text or the supplementary materials. The code from this work is available at https://github.com/zhoutopo/science_aging_model and Zenodo (*51*). **License information**: Copyright © 2023 the authors, some rights reserved; exclusive licensee American Association for the Advancement of Science. No claim to original US government works. https://www.science.org/about/science-licenses-journal-article-reuse

SUPPLEMENTARY MATERIALS

science.org/doi/10.1126/science.add7631
Materials and Methods
Figs. S1 to S19
Tables S1 to S4
References (*52*–*58*)
MDAR Reproducibility Checklist
Movie S1

View/request a protocol for this paper from *Bio-protocol*.

Submitted 1 July 2022; accepted 3 March 2023
10.1126/science.add7631